6th European Conference on Computational Mechanics (ECCM 6)
7th European Conference on Computational Fluid Dynamics (ECFD 7)
1115 June 2018, Glasgow, UK

MODEL ORDER REDUCTION IN VISCOPLASTIC FLOW MODELLING USING PROPER ORTHOGONAL DECOMPOSITION AND NEURAL NETWORKS

EKATERINA A. MURAVLEVA[1], IVAN V. OSELEDETS[1] AND DMITRY A. KOROTEEV[1]

[1] Skolkovo Institure of Science and Technology
Postal address
e-mail address and URL

Key words: Machine learning, viscoplastic flows, neural networks,, proper orthogonal decomposition

Abstract. This document provides information and instructions for preparing a Full Paper to be included in the Proceedings of *ECCM ECFD 2018 Conference*.

e present a method to construct reduced-order models for duct flows of Bingham media. Our method is based on proper orthogonal decomposition (POD) to find a low-dimensional approximation to the velocity and artificial neural network to approximate the coefficients of a given solution in the constructed POD basis. We use well-established augmented Lagrangian method and finite-element discretization in the "offline" stage. We show that the resulting approximation has a reasonable accuracy, but the evaluation of the approximate solution several orders of magnitude times faster.

1 Introduction

Yield stress fluid flows play an important role in many applications, especially in the oil and gas industry [FPdSM17]. There are several areas within petroleum industry where viscoplasticity is considered as a key mechanism or an enabler for technologies aimed at enhancing oil or gas production. Hydraulic Fracturing (HF) [YW14] operation is invented to stimulate fluid inflow from near wellbore reservoir to a well. It is performed by pumping fluid into a well at a high pressure so that it initiates fracture(s) in near wellbore formation. Fracturing fluid is designed in a various forms depending on specifics of the wellbore and the formation. In some specific cases the fluid is made to be viscoplastic. Paper [BK$^+$74] refers to a foam fracturing and authors consider viscoplasticity of the foam as one of the key factors of fracturing job success. One of the key challenges of the whole petroleum industry are viscoplastitity of emulsions forming in porous space of oil reservoirs at contacts between oil and water[MYM06]. These regions are among top factors limiting the oil recovery factor. As an example, [SZ15] is a paper devoted to study on how to break and recover such emulsions. These emulsion treatment approaches are considered to be one of the most efficient methods for enhanced oil recovery at a reservoir

scale. Another approach to enchancing oil recovery is viscoplastic diverters [OAG+13] which are used as a tools for re-distributing multiphase flows in porous rocks and, in particular, hydrocarbon reservoirs [Eze14].

Viscoplastic flow modeling is often computationally expensive, see recent reviews [SW17], [MT17]. The main difficulty in design of appropriate solution techniques is related to the non-differentiability of the constitutive relations. Over the past 40 years, two main family of methods were suggested in the literature: the so-called regularization approach and augmented Lagrangian method (ALM). We choose the last one since it is typically more robust and reliable. It consists of an outer iterative process and on each step of this process we need to solve a boundary-value problem. In this paper we apply reduced order modeling and machine learning techniques to approximate the results of numerical simulations of viscoplastic media. The idea is that the physical system is described by a few number of input parameters (i.e. Bingham number), but the numerical simulation requires the computation of the solution in each grid cell, thus the complexity is high. Our goal is to compute the approximation to the solution by learning from the results of numerical simulations for different values of parameters, describing the system.

The computation is split into two steps. At the first step (which is also called *offline stage*) we conduct numerical simulation for different values of parameters and collect solutions (so-called *snapshots*). This step is computationally expensive and is typically done using high-performance computing. Based on the result of numerical simulation we compute the approximant, which can be computed efficiently for any new value of parameters in the *online stage*. Although this is a standard framework in the field of reduced order modeling, application of these methods to numerical simulation of viscoplastic media faces several challenges which we address. The main challenge is that the equations are nonlinear, and even it is quite straightforward to reduce the dimensionality of the problem using *proper orthogonal decomposition* (POD), it is not simple to construct the approximant that is easy to evaluate for new parameter values. In order to solve this problem, we introduce an additional approximant, which is based on artificial neural networks (ANN) and is learned using standard backpropagation techniques. To summarize, main contributions of our paper are:

- We propose a "black-box" approach to construct a reduced-order model for Bingham fluid flow in a channel based on POD to compute a low-dimensional projection, and ANN to approximate the coefficients of POD decomposition from the parameters
- We show the accuracy of the proposed approximation for a single yield stress for different domains
- We show the accuracy of the proposed approximation for piecewise-constant yield stress limit
- Our method allows to achieve several orders of magnitude speedup for the considered examples

2 Test problem

2.1 Governing equations

The constitutive relations of viscoplastic Bingham medium connect the viscous stress tensor $\boldsymbol{\tau}$ to the rate-of-strain tensor $\dot{\boldsymbol{\gamma}}$ as follows:

$$\dot{\boldsymbol{\gamma}} = 0, \quad |\tau| \leq \tau_s$$
$$\boldsymbol{\tau} = \left(\frac{\tau_s}{|\dot{\gamma}|} + \mu\right)\dot{\boldsymbol{\gamma}}, \quad |\tau| > \tau_s$$

where μ is the plastic viscosity, τ_s is the yield stress limit, $\mathbf{u}$ is the velocity vector, $\dot{\boldsymbol{\gamma}} = \nabla\mathbf{u} + (\nabla\mathbf{u})^\top$, and the norms of the tensors

$$|\dot{\boldsymbol{\gamma}}| = \sqrt{\dot{\boldsymbol{\gamma}} : \dot{\boldsymbol{\gamma}}}, \quad |\boldsymbol{\tau}| = \sqrt{\boldsymbol{\tau} : \boldsymbol{\tau}}$$

As a test problem, we consider well-known Mosolov problem [MM65, MM66, MM67]. It describes an isothermal steady laminar flow of an incompressible Bingham fluid in an infinitely long cylinder pipe with a cross-section $\Omega \subset \mathbb{R}^2$ under the action of the pressure gradient. It is modeled by the following equation

$$-\mu\nabla^2 u - \tau_s \nabla \cdot \left(\frac{\nabla u}{|\nabla u|}\right) = f, \quad u_{\partial\Omega} = 0 \tag{1}$$

which follows from mass and momentum conservation laws. We consider the no-slip (Dirichlet) boundary conditions. Here u is the axial velocity ($\mathbf{u} = (0, 0, u)$), f is constant pressure gradient. After proper rescaling, we can obtain the dimensionless form of the problem (1) with the Bingham number B as a parameter:

$$-\nabla^2 u - B\nabla \cdot \left(\frac{\nabla u}{|\nabla u|}\right) = 1, \quad u_{\partial\Omega} = 0 \tag{2}$$

This problem has been solved numerically in many papers (both for steady [SR04, MGA04, HY05, Mur09] and unsteady [MM09, MMGM10] cases). Wall slip boundary conditions were considered in [RS08, DPKG14, DG14].

2.2 Numerical methodology

The solution of the Mosolov problem can be found from the minimization of the functional

$$J(u) = \int \left(\frac{1}{2}|\nabla u|^2 + B|\nabla u| - fu\right) dx \to \min_{u \in H_0^1(\Omega)}. \tag{3}$$

Of the most efficient and widely-used approaches to solve (3) is the augmented Lagrangian method (ALM) [FG83], which has the following form. First, we introduce an additional variable $\mathbf{q} = \nabla u$ and consider constrained minimization problem

$$\min_{u, \mathbf{q}=\nabla u} J(u, \mathbf{q}), \quad J(u, \mathbf{q}) = \int \left(\frac{1}{2}|q|^2 + B|q| - fu\right) dx.$$

To deal with the constraint, the Lagrange multiplier $\boldsymbol{\lambda}$ is introduced, and also a penalty term is added, thus leading to the augmented Lagrangian

$$\mathcal{L}_r = \int \left(\frac{1}{2}|q|^2 + B|q| - fu \right) dx + \int \boldsymbol{\lambda} \cdot (\mathbf{q} - \nabla u) dx + \frac{r}{2} \int |\boldsymbol{\lambda} - \nabla u|^2 dx. \tag{4}$$

The original minimization problem (3) is equivalent to finding a saddle point of the functional (4). For finding the saddle point of (4) we use the ALG2 method [FG83]. Given an initial approximation $u^{(k)}, \mathbf{q}^k, \boldsymbol{\lambda}^k$ we compute the next approximation by the following steps

- (Update u) Solve

$$-r\Delta u^{(k+1)} = f - r\nabla \cdot \mathbf{q}^k - \nabla \cdot \boldsymbol{\lambda}^k. \tag{5}$$

- (Update $\mathbf{q}$)

$$\mathbf{q}^{(k+1)}(\mathbf{x}) = \begin{cases} 0, & \text{if} \quad |\boldsymbol{\lambda}^k(\mathbf{x}) + r\nabla u^{(k+1)}(\mathbf{x})| \leq B, \\ \frac{\boldsymbol{\lambda}^k(\mathbf{x}) + r\nabla u^{(k+1)}(\mathbf{x})}{1+r} \left(1 - \frac{B}{|\boldsymbol{\lambda}^k(\mathbf{x}) + r\nabla u^{(k+1)}(\mathbf{x})|} \right), & \text{otherwise} \end{cases} \tag{6}$$

- (Update $\boldsymbol{\lambda}$)

$$\boldsymbol{\lambda}^{(k+1)} = \boldsymbol{\lambda}^{(k)} + \rho \left(\mathbf{q}^{(k+1)} - \nabla u^{(k+1)} \right). \tag{7}$$

To implement (5), (6), (7) numerically, we use weak formulations for each of these problems and finite element method (FEM). We use FENICS package [LMW12] for the implementation, where only weak formulation of the problem is necessary, and everything else (including unstructured mesh generation) is done automatically. We used standard finite element spaces: for velocity we used piecewise-linear functions, and for $\mathbf{q}$ and $\boldsymbol{\lambda}$ – piecewise-constant functions. Given the solver (which consists of executing steps (5), (6), (7) until convergence), we can now focus on the main problem considered in this paper: the construction of the reduced model.

3 Dimensionality reduction

A standard approach to the construction of reduced models is the linear dimensionality reduction [KV02, Pet89, LMQR14].Let $u_h(p) \in R^N$ be the numerical solution of the problem (2). The idea of the POD method is to construct the approximation of the form

$$u_h(p) \approx \widehat{u}_h = \sum_{\alpha=1}^{r} v_\alpha d_\alpha(p), \quad v_\alpha \in \mathbb{R}^N, \tag{8}$$

where v_α are POD basis functions, $d_\alpha(p)$ are the coefficients of the POD model and r is the dimension of the reduced model. The first step is to compute *snapshots*, i.e., specific solutions $u_h(p_i), \quad i = 1, \ldots, K$ for different parameter values. The selection of snapshots

is an independent research question. In our case, we sample the parameter space using random or quasi-random number generator. These solutions are organized into an $N \times K$ matrix

$$U = \begin{bmatrix} u_h(p_1) & \dots u_h(p_K) \end{bmatrix}.$$

Looking at the singular values of this matrix we can decide what is the appropriate dimension for the reduced model. A typical criteria gives the reduced dimension

$$r = \min\{k : \sum_{s=k+1}^{P} \sigma_s^2 \leq \epsilon^2\},$$

where σ_s are singular values of U and ϵ is the required accuracy of the approximation. In this case, we approximate the data matrix by the truncated singular value decomposition

$$U \approx W \Lambda C, \tag{9}$$

where W is an $N \times r$ matrix with orthonormal columns, Λ is an $r \times r$ diagonal matrix with singular values on the diagonal and C is the coefficient matrix. From (9) the following reduced model follows:

$$u_h(p) \approx \widehat{u}_h = \sum_{\alpha=1}^{r} \sigma_\alpha w_\alpha c_\alpha(p), \tag{10}$$

The difference between (10) and (8) is only in the normalization of the basis functions, which allows to sort them with respect to their importance, which is measured by singular values. The idea of POD is that most of the solution can be captured with $r \ll N$ modes, thus every solution can be efficiently represented with r parameters instead of N in the original discrete model. However it is not the compression that is important, but also the computation of the approximation given the new parameter p_* which was not in the training set. Here we need to compute the coefficients $c_\alpha(p)$. One of the approaches is to write the equations directly it terms of the coefficients $c_\alpha(p)$. Unfortunately, even the computation of the energy functional can not be simplified, so the computation of these coefficients directly from the original formulation is as costly, as the solution of the full problem. Thus, we propose to approximate each coefficient in (10) directly:

$$c_\alpha(p) \approx \widehat{c}_\alpha(p).$$

This gives another approximant to the solution:

$$u_h(p) \approx \widehat{u}_h(p) \approx \widetilde{u}_h(p) = \sum_{\alpha=1}^{r} \sigma_\alpha w_\alpha \widehat{c}_\alpha(p).$$

Since w_α are orthonormal, error of this approximation consists of two parts. First is the error of linear dimensionality reduction and second is the error of coefficient approximation, which also influences the final error. It is natural to make them of the same size.

Moreover, c_α for different α have to be approximated with different accuracy. Indeed, we have

$$\|\widehat{u}_h(p) - \widetilde{u}_h(p)\| = \sum_{\alpha=1}^{r} \sigma_\alpha^2 (c_\alpha - \widehat{c}_\alpha)^2,$$

thus to get approximation error of order ϵ it is sufficient to have

$$|c_\alpha - \widehat{c}_\alpha| \leq \frac{\epsilon}{\sigma_\alpha \sqrt{r}},$$

i.e. coefficients, corresponding to POD modes with smaller singular values, can be approximated with lower accuracy. This is important since the higher is the mode number, the more oscillatory behavior it describes and the approximation of the coefficient is less accurate. But it does not create any problems since we do not need these coefficients with high accuracy.

4 Approximation of POD coefficients using ANN

To approximate the coefficient we suggest to use artificial neural networks (ANN), and the coefficients are learned directly from the data. ANN are often used to approximate complex multiparametric dependencies, and can be written as a superposition of linear transformations (parametrized by weight matrices) and simple point-wise nonlinear functions (also known as activation function). Convolutional neural networks (CNN) have gained a lot of attention recently and show tremendous success in the area of computer vision, image processing, text mining. In this paper, the input has a small dimension, so CNN are not directly applicable. Instead, we focus on classical fully-connected networks, which can be written in the form (for simplicity, we omit the index α and illustrate the model in a 3-layer case)

$$c(p) \approx \widehat{c}(p) = f(W_3 f(W_2 f(W_1 p + b_1) + b_2) + b_3),$$

where p is a parameter vector, $W_k, k = 1, \dots 3$ are weight matrices of size $H_{k-1} \times H_k$, and b_k are biases. Also we have $H_0 = P, \quad H_3 = 1$. The numbers H_k correspond to the number of neurons in the hidden layer. Activation function f is applied to each element of the vector, for example, at the first step, to the vector $W_1 p$. A typical choice for $f(x)$ is the ReLU activation of the form

$$f(x) = \begin{cases} x, & x > 0, \\ 0, & x \leq 0. \end{cases}$$

Another option is the function $f(x) = \tanh(x)$. ANN parameters are learned by minimizing the loss between predicted and observed coefficients:

$$\sum_{j=1}^{M} \left(c(p_j) - \widehat{c}(p_j)\right)^2 \to \min.$$

The solution of the optimization problem is done using the standard gradient optimization methods (based on backpropagation [RHW88]) available in modern machine learning frameworks. In our implementation we have used Keras python library [C+15] with a Tensorflow backend.

5 Numerical results

5.1 Single yield stress limit

As our first example, we consider a single-parameter case, namely, parameter is the Bingham number B. We examine several types of cross-sections: square, circle, rectangle, triangle, L-shaped domain. We sample Bingham numbers from 0 to 1 to obtain snapshots. Note that for all these domains the critical yield stress is lower, so for $B > B_{crit}$ the velocity is equal to 0, and snapshots, corresponding to these parameters do not provide any additional information. Such behavior is automatically captured by the proposed algorithm. For each domain, we collect the snapshot matrices, compute first POD basis functions, and corresponding coefficients. Singular values of the snapshot matrices decay very fast (see Figure 1), and $K = 20$ provide very high accuracy of the approximation. The first basis functions for different domains are shown on Figure 2.

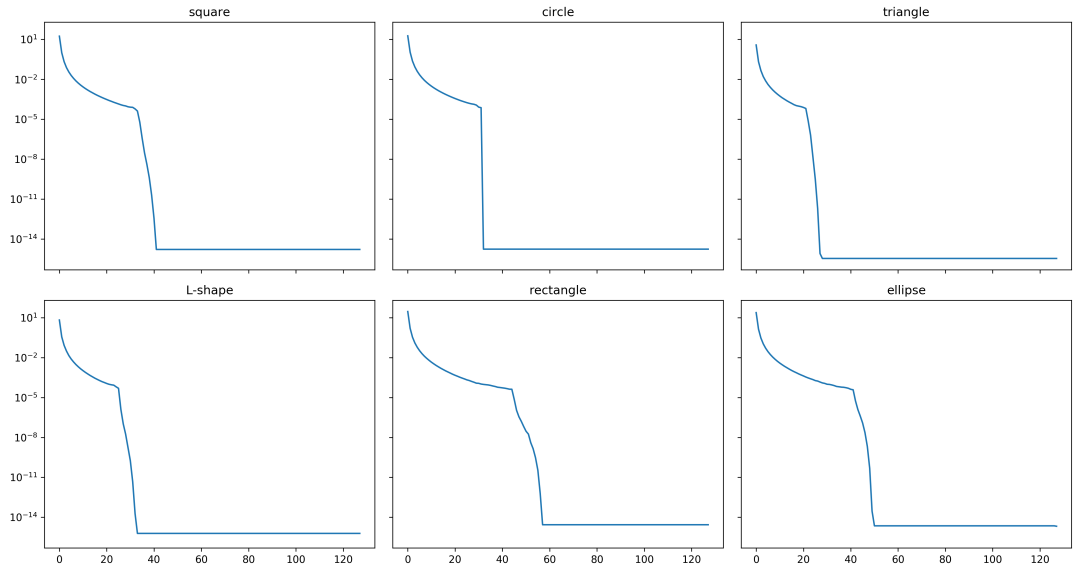

Figure 1: Singular values of the snapshot matrices for different domains

.

As we see, the singular values decay very fast, thus it is sufficient to leave at most $K = 20$ coefficients to get a good approximation. The first 5 basis functions and corresponding singular values are shown in Figure 2.

To construct a neural network approximation for the mapping from B to the first K coefficients of the POD decomposition, we randomly split the dataset into test and train parts (33% test and 67% train), and learn a corresponding mapping. As an architecture

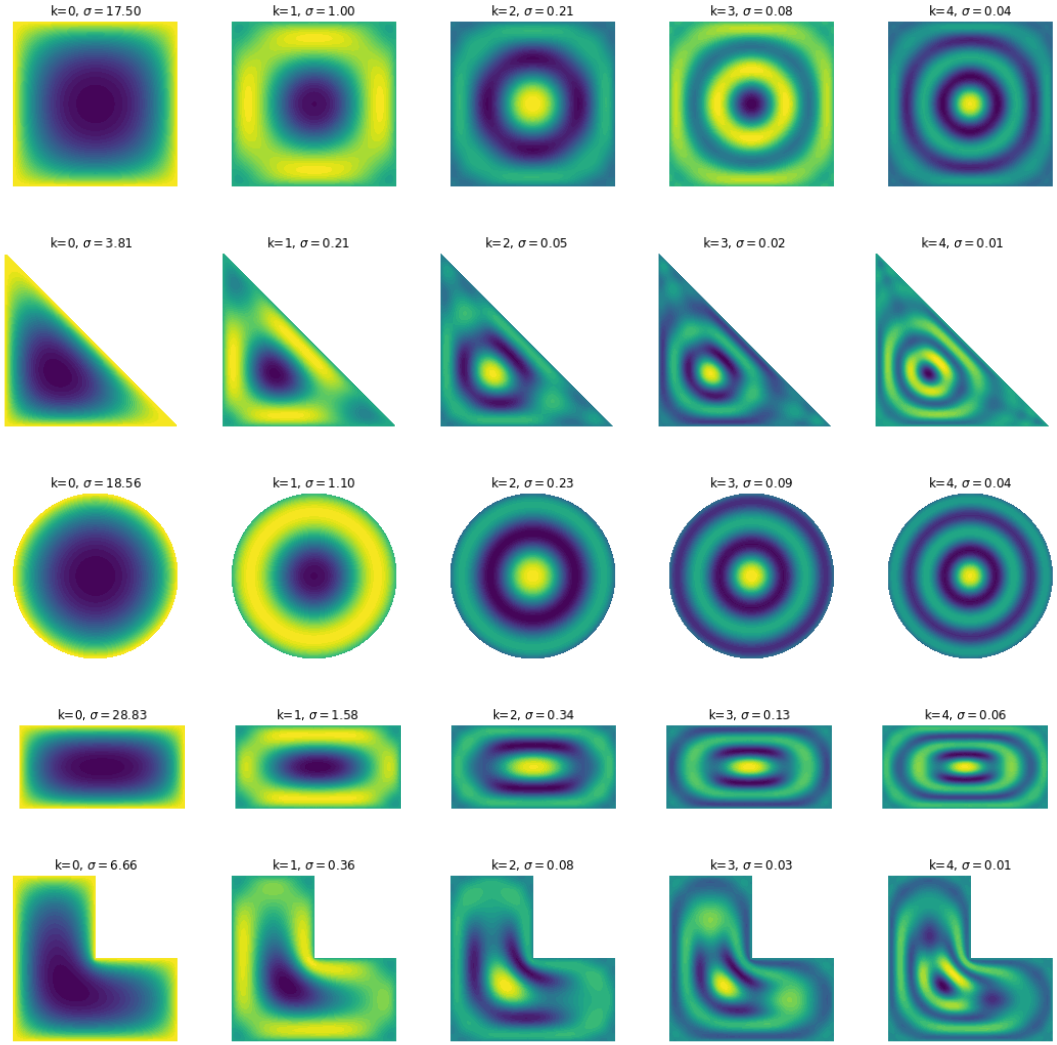

Figure 2: First 5 POD basis functions for different domains

of ANN we take 3 hidden layers with $60, 50, 40$ hidden units, respectively and one output layer. As an optimizer, ADAM optimizer [KB14] was used with default parameters. The relative error of approximation on the test set for different domains is given in Table 1. This error is defined as as sum over all test samples, divided by the sum of all coefficients:

$$\varepsilon_{test} = \sqrt{\frac{\sum_{i=1}^{N_{test}} \sum_{k=1}^{K} \left(c_k^{(i)} - \widehat{c}_k^{(i)}\right)^2}{\sum_{i=1}^{N_{test}} \sum_{k=1}^{K} (c_k^{(i)})^2}}.$$

5.2 Non-homogenious yield stress limit

We consider the square case ($\Omega = [-\frac{1}{2}, \frac{1}{2}]^2$), and a piecewise-constant yield stress limit. This corresponds to the flow of different fluids with different yield stress limits. This

Domain	Relative error
square	0.006686
circle	0.006325
triangle	0.005700
L-shape	0.008667
rectangle	0.005344
ellipse	0.003489

Table 1: Relative error in the L_2 norm for the approximation of the first $K = 200$ coefficients of the POD decomposition (test set).

type of flows is rather common in practice: it includes such processes as lamination, coextrusion and deposition. For the model problem we consider a two-parameter problem with piecewise-constant $B(x_1, x_2)$:

$$B(x_1, x_2) = \begin{cases} B_1 & x_1 \leq 0, \\ B_2 & x_1 > 0. \end{cases}$$

The parameters B_1 and B_2 vary from 0 to 0.8. For this problem we need to select more snapshots than for a single stress limit to get similar accuracy. We also have to sample two-dimensional points in the parameter space. To generate the POD basis, we compute 500 snapshots with B_1 and B_2 generated using Halton quasi-random sequence generator [Nie92]. The decay of singular values of the snapshot matrix is shown on Figure 3, and several first singular vectors are depicted on Figure 4. Then we split the dataset randomly into training (67% points) and and testing (33% points), and fit a fully connected ANN to map two input parameters (B_1 and B_2) to the first $K = 20$ coefficients of the POD decomposition. As an architecture of ANN we take 3 hidden layers with $60, 50, 40$ hidden units, respectively and one output layer.

As an optimizer we again use the Adam optimizer with default parameters. The relative error for the approximation of the first $K = 20$ coefficients is 0.008 on the test set.

The main benefit of using the reduced model is that computing the approximate solution for new B_1, B_2 is very fast. The final model takes approximately 4 milliseconds to evaluate, whereas the full FEM model takes 45 seconds. The comparison of two solutions is given on Figure 5 for $B_1 = 0.25$ and $B_2 = 0.05$.

6 Conclusions and future work

We have presented a general approach for the construction of reduced models of Bingham fluid flows in the simplest possible case – channel (duct) flow. Although being model, these flows share the main characteristics of more general cases. The proposed method is "easy to implement": all the steps are automatic (generation of snapshots and fitting a neural network), but difficult to analyze: there is no guarantee that the approximated solution will share important properties of the original solution, such as positivity. This

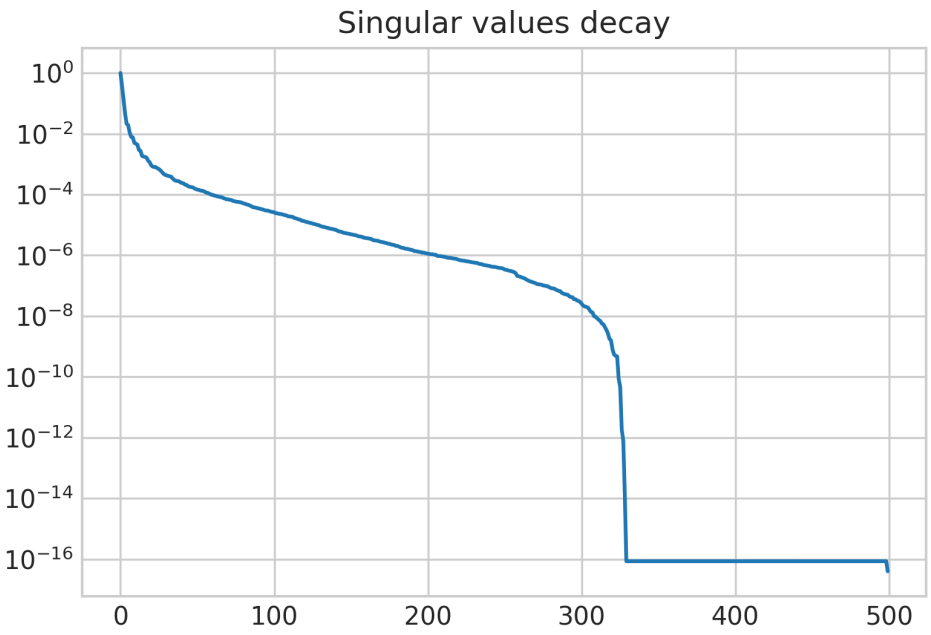

Figure 3: Decay of singular values for two-parameter problem

.

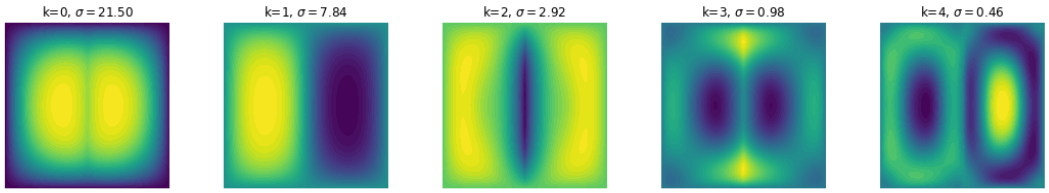

Figure 4: First five POD basis functions

.

requires a separate study, as well as the application of the constructed reduced-order model to real-life design problems.

REFERENCES

[BK+74] R.E. Blauer, C.A. Kohlhaas, et al. Formation fracturing with foam. In *Fall meeting of the society of petroleum engineers of AIME*. Society of Petroleum Engineers, 1974.

[C+15] François Chollet et al. Keras, 2015.

[DG14] Y. Damianou and G.C. Georgiou. Viscoplastic poiseuille flow in a rectangular duct with wall slip. *J. Non-Newtonian Fluid Mech.*, 214:88–105, 2014.

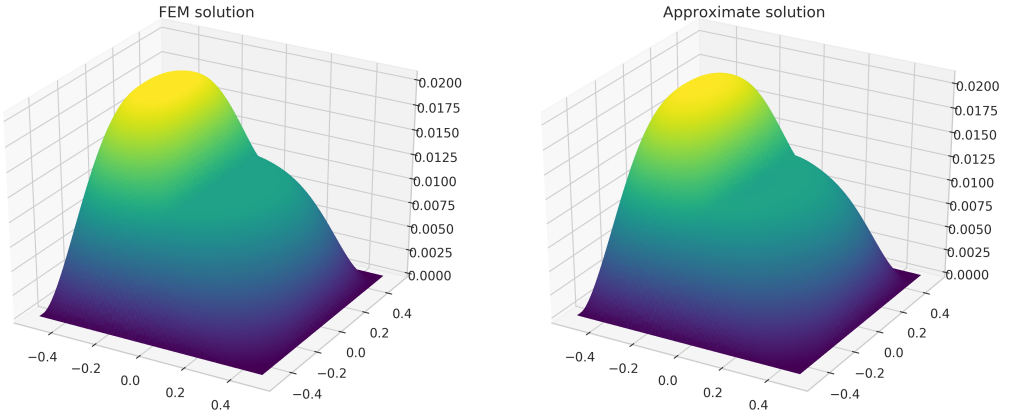

Figure 5: Comparison of FEM and approximate solution

.

[DPKG14] Y. Damianou, M. Philippou, G. Kaoullas, and G.C. Georgiou. Cessation of viscoplastic poiseuille flow with wall slip. *J. Non-Newtonian Fluid Mech.*, 203:24–37, 2014.

[Eze14] R.G. Ezell. Treatment fluids comprising transient polymer networks, November 18 2014. US Patent 8,887,809.

[FG83] M. Fortin and R. Glowinski. The augmented Lagrangian method, 1983.

[FPdSM17] I. A. Frigaard, K.G. Paso, and P.R. de Souza Mendes. Binghams model in the oil and gas industry. *Rheologica Acta*, 56(3):259–282, 2017.

[HY05] R. Huilgol and Z. You. Application of the augmented lagrangian method to steady pipe flows of bingham, casson and herschelbulkley fluids. *Journal of Non-Newtonian Fluid Mechanics*, 128(2-3):126–143, 2005.

[KB14] D. Kingma and J. Ba. Adam: A method for stochastic optimization. *arXiv preprint arXiv:1412.6980*, 2014.

[KV02] K. Kunisch and S. Volkwein. Galerkin proper orthogonal decomposition methods for a general equation in fluid dynamics. *SIAM Journal on Numerical analysis*, 40(2):492–515, 2002.

[LMQR14] T. Lassila, A. Manzoni, A. Quarteroni, and G. Rozza. Model order reduction in fluid dynamics: challenges and perspectives. In *Reduced Order Methods for modeling and computational reduction*, pages 235–273. Springer, 2014.

[LMW12] A. Logg, K.A. Mardal, and G.N. Wells. *Automated Solution of Differential Equations by the Finite Element Method*. Springer, 2012.

[MGA04] M. A. Moyers-Gonzalez and Frigaard I. A. Numerical solution of duct flows of multiple visco-plastic fluids. *Journal of Non-Newtonian Fluid Mechanics*, 122(1-3):227–241, 2004.

[MM65] P.P. Mosolov and V.P. Miasnikov. Variational methods in the theory of the fluidity of a viscous-plastic medium. *Journal of Applied Mathematics and Mechanics*, 29(3):545–577, 1965.

[MM66] P.P. Mosolov and V.P. Miasnikov. On stagnant flow regions of a viscous-plastic medium in pipes. *Journal of Applied Mathematics and Mechanics*, 30(4):841–854, 1966.

[MM67] P.P. Mosolov and V.P. Miasnikov. On qualitative singularities of the flow of a viscoplastic medium in pipes. *Journal of Applied Mathematics and Mechanics*, 31(3):609–613, 1967.

[MM09] EA Muravleva and LV Muravleva. Unsteady flows of a viscoplastic medium in channels. *Mechanics of solids*, 44(5):792–812, 2009.

[MMGM10] Larisa Muravleva, Ekaterina Muravleva, Georgios C Georgiou, and Evan Mitsoulis. Numerical simulations of cessation flows of a bingham plastic with the augmented lagrangian method. *Journal of Non-Newtonian Fluid Mechanics*, 165(9):544–550, 2010.

[MT17] E. Mitsoulis and J. Tsamopoulos. Numerical simulations of complex yield-stress fluid flows. *Rheologica Acta*, 56(3):231–258, 2017.

[Mur09] E.A. Muravleva. Finite-difference schemes for the computation of viscoplastic medium flows in a channel. *Mathematical Models and Computer Simulations*, 1(6):768–279, 2009.

[MYM06] K. Moran, A. Yeung, and J. Masliyah. The viscoplastic properties of crude oil–water interfaces. *Chemical engineering science*, 61(18):6016–6028, 2006.

[Nie92] H. Niederreiter. *Random number generation and quasi-Monte Carlo methods*. SIAM, 1992.

[OAG+13] M. Ocalan, F. M. Auzerais, P. Ganguly, A. Robisson, and J. Pabon. Apparatus and method for treating a subterranean formation using diversion, September 24 2013. US Patent 8,540,015.

[Pet89] J. S. Peterson. The reduced basis method for incompressible viscous flow calculations. *SIAM Journal on Scientific and Statistical Computing*, 10(4):777–786, 1989.

[RHW88] D.E. Rumelhart, G.E. Hinton, and R.J. Williams. Learning representations by back-propagating errors. *Cognitive modeling*, 5(3):1, 1988.

[RS08] Nicolas Roquet and Pierre Saramito. An adaptive finite element method for viscoplastic flows in a square pipe with stick–slip at the wall. *Journal of Non-Newtonian Fluid Mechanics*, 155(3):101–115, 2008.

[SR04] P. Saramito and N. Roquet. An adaptive finite element method for viscoplastic fluid flows in pipes. *Journal of Non-Newtonian Fluid Mechanics*, 190(40-41):5391–5412, 2004.

[SW17] P. Saramito and A. Wachs. Progress in numerical simulation of yield stress fluid flows. *Rheologica Acta*, 56(3):211–230, 2017.

[SZ15] G. Sun and J. Zhang. Structural breakdown and recovery of waxy crude oil emulsion gels. *Rheologica Acta*, 54(9-10):817–829, 2015.

[YW14] C. H. Yew and X. Weng. *Mechanics of hydraulic fracturing*. Gulf Professional Publishing, 2014.